Translational

# Laser-Mediated Activation of Human Retinal Pigment Epithelial Cells and Concomitant Release of Matrix Metalloproteinases

*Jin Jun Zhang,*[1,3] *Yue Sun,*[2,3] *Ali A. Hussain,*[1] *and John Marshall*[1]

**Purpose.** To investigate cellular dynamics and associated matrix metalloproteinase (MMP) release patterns of human retinal pigment epithelium (RPE) cells subsequent to irradiation by nanosecond pulsed laser at energy levels below visual threshold.

**Methods.** Following a stabilization period, human RPE-Bruch's-choroid explants were irradiated with a nanosecond laser system (Q-switched, frequency doubled YAG laser, 532 nm), using a 400 μm spot size with a discontinuous energy distribution and total irradiance of 240 mJ/cm$^2$, and returned to the incubator for a further 14 days. RPE cellular dynamics were assessed using confocal laser scanning, conventional microscopy, cell viability, and proliferation assays. MMPs were quantified by gelatine zymography and densitometry.

**Results.** Within 4 hours of laser intervention, 47% ± 8% (mean ± SEM, $n = 6$) of the RPE cells within the treatment zone showed clear signs of injury. By posttreatment days 10 to 14, most of the injured beds were repopulated by migrating RPE cells from regions surrounding the lesion. Release of inactive MMP-2 was little altered over the 2-week experimental period, whereas levels of inactive MMP-9 increased 1.3-fold by day 1 to reach a 2.8-fold threshold by day 7 ($n = 4$; $P < 0.05$). However, changes in activated MMP-2 and MMP-9 were much more profound with levels increasing 6.7 ± 2.6-fold (mean ± SEM, $n = 6$; $P < 0.001$) and 4.4 ± 1.1-fold (mean ± SEM, $n = 5$; $P < 0.01$), respectively, above controls at day 7 post laser.

**Conclusions.** The nanosecond laser pulse modality provides an avenue for transiently increasing the RPE-mediated release of active MMP enzymes. The likely impact of this enzymatic release on the structural and functional aspects of aging Bruch's membrane requires further evaluation. (*Invest Ophthalmol Vis Sci.* 2012;53:2928–2937) DOI:10.1167/iovs.11-8585

Aging of Bruch's membrane is characterized by progressive thickening, accumulation of various lipid-rich extracellular matrix (ECM) deposits, increased matrix cross-links, and accumulation of advanced glycation- and lipid-end products (AGEs and ALEs).[1–4] In advanced aging associated with ARMD, such changes are exaggerated leading to the demise of retinal pigment epithelial (RPE) and photoreceptor cells mediated by processes of apoptosis, inflammation (involving Complement Factor H) and/or neovascular episodes via VEGF.[5,6]

The structural and molecular changes of aging Bruch's were hypothesized to interfere with the transport functions of the membrane for the delivery of nutrients and removal of waste products to and from the RPE/retina and the choroidal circulation.[7,8] Our functional studies have confirmed the above hypothesis of an age-related deterioration in transport processes across Bruch's and provided an etiological mechanism for progression toward early ARMD.[9–13]

Most ECMs undergo continuous remodeling by tightly coupled processes of degradation and synthesis thereby maintaining their functional integrity. In Bruch's membrane, the increased deposition of normal ECM material is indicative of ongoing synthesis, but the simultaneous accumulation of denatured or insoluble collagen, amounting to nearly 50% of total collagen in the aged, suggests problems with the degradation process.[3]

The degradation pathway for ECM turnover comprises the family of matrix metalloproteinases (MMPs) together with their inhibitors (TIMPs). Among the family, MMP-2 and MMP-9, highly conserved $Zn^{2+}$- and $Ca^{2+}$-dependent extracellular peptidases, can degrade most ECM components and many non-ECM molecules allowing for matrix turnover.[14] Such activity can also promote cell migration and modulation of biologically active molecules by direct cleavage or by release from ECM stores.[15,16] Most MMPs are secreted by the RPE as latent zymogens, achieving catalytic properties in the ECM milieu. Some MMPs are processed intracellularly, whereas a few are processed at the cell membrane into fully active enzymes.[17]

MMP-2 and MMP-9 have previously been demonstrated in Bruch's membrane and the level of inactive proenzymes was shown to increase with age[18]; however, the same study highlighted the low or undetectable level of active forms of MMPs and this observation may underlie the reduced degradation capacity in aged eyes. The advanced ageing in ARMD was also associated with significantly reduced levels of active MMP-2 and MMP-9.[19] In vitro, the introduction of activated MMPs into donor human Bruch's was associated with significant functional improvement in its transport properties.[20] These results demonstrate the potential for using the MMP pathway as a therapeutic avenue for addressing the aging decline in transport across Bruch's and thereby slow or reverse the progression of ARMD. The key to intervention depends on providing a method for increasing the level of activated MMPs within Bruch's membrane.

Early laser photocoagulation studies for diabetic maculopathy had often observed drusen regression in surrounding

From the [1]Division of Molecular Therapy, UCL Institute of Ophthalmology, London, United Kingdom; and the [2]Department of Ophthalmology, Ruijin Hospital, Shanghai Jiao Tong University, China.

[3]These authors contributed equally to the work presented here and should therefore be regarded as equivalent authors.

Supported by Fight for Sight UK and the National Institute for Health Research Biomedical Research Centre for Ophthalmology.

Submitted for publication October 3, 2011; revised February 12, 17, and 28, 2012; accepted March 11, 2012.

Disclosure: **J.J. Zhang**, None; **Y. Sun**, None; **A.A. Hussain**, None; **J. Marshall**, None

Corresponding author: Jin Jun Zhang, Division of Molecular Therapy, UCL Institute of Ophthalmology, 11–43 Bath Street, London EC1V 9EL, UK; jj.zhangopth@gmail.com.

areas of the lesion.[21] The underlying mechanism may be related to the release of activated MMPs by migrating RPE cells as part of the wound-healing process.[20] Following on from Gass' observations,[21] several groups using conventional lasers have attempted to reduce drusen density as a prophylactic treatment for ARMD.[22,23] Despite the partial removal of drusen, they observed no real improvement in vision or in the natural history of the disease. Several possibilities may be responsible for this unexpected shortfall. First, there is no correlation in the density of druse and retinal sensitivity suggesting that diffuse deposits within Bruch's rather than focal drusen are responsible for poor retinal function.[24,25] It is not known whether the diffuse deposits were altered by the laser regimes. Second, the photocoagulation regime used too few lesions and they were placed too far from the macular region, based on a risk versus benefit assessment. The reason for adopting this regime was that conventional lasers with millisecond exposures produced damaging heat flow transients up to 150 μm from the laser lesion, damaging both overlying photoreceptors and underlying Bruch's and choroidal structures, and thereby increasing the risk of secondary choroidal neovascularisation.[26,27] Similarly, subthreshold laser energy levels (with either Argon green (514 nm) or diode (810 nm) delivered with 100 millisecond pulses were also associated with increased risk of choroidal neovascularization.[28–30]

The so-called "micro" pulse lasers using pulse durations in the microsecond range restrict these heat transients to 30 μm. The newly introduced true short-pulse lasers, by emitting a series of laser pulses of in the submicrosecond and nanosecond domain, restrict heat flow to within 1 to 3 μm of melanin granules and produce RPE effects without damaging Bruch's or photoreceptors by primary mechanisms of "bubble" formation and its rapid expansion.[31–39] Because these short-pulse lasers specifically target RPE cells without damage to photoreceptors or Bruch's, we suggest that they could allow therapeutic access to the entire macular region.[40] However, this modality will damage all RPE cells in the irradiation zone, and because photoreceptors depend on the RPE for metabolic supply, those at the center of the lesion will be compromised until the wound closes and may therefore suffer secondary damage. This can be minimized by the use of a discontinuous or speckled laser beam profile so that RPE cells are damaged in a randomized patchwork within the lesion, thereby allowing rapid wound closure and reducing the time over which photoreceptors remain without metabolic support by the RPE.[41]

The purpose of the current study was to assess the potential for laser-activated release of MMPs by RPE cells and their involvement in rejuvenating the transport pathways across the RPE-Bruch's membrane complex. Here we report the initial results of the impact of a 3-ns pulsed laser (532 nm) on human RPE migration and associated alterations in the release patterns of MMP enzymes (MMP-2 and MMP-9).

## Methods

### Establishment of Human RPE-BC Explants

Human donor eyes (with corneas removed for transplantation) were obtained from the Bristol Eye Bank (Bristol, UK). The eyes (donor age range: 21–72 years; postmortem times <48 hours; $n = 60$) were dissected immediately on arrival in the laboratory. We have previously shown structural and functional stability of Bruch's for up to the 50 hours postmortem time examined.[9] Similarly, the functional stability of human RPE was assessed by monitoring the high-affinity active uptake of the amino acid taurine, and this was observed to be unaltered up to 76 hours of postmortem time.[42]

Having carefully removed the neurosensory retina, two adjacent 10-mm trephines were obtained overlapping the macular region followed by blunt dissection to isolate the RPE-Bruch's-choroid complex (RPE-BC). One of these acted as the control, whereas the other was irradiated.

The tissue discs were then mounted in a specially designed culture chamber with an optical window to allow visualization of the cells and to facilitate laser treatment during in vitro culture (Fig. 1). Once mounted, a central 4-mm-diameter of the RPE monolayer was sealed from the surrounding tissues and exposed to the medium.

The compartment of the culture chamber was filled with fetal calf serum (FCS; Gibco-Invitrogen, Paisley, UK) and incubated overnight at 37°C in a humidified atmosphere containing 5% $CO_2$. Following this initial stabilization period, the serum was carefully aspirated and replaced with an equal volume of HEPES-buffered Dulbecco's modified Eagle's medium/Ham's F-12 (50:50 mixture), supplemented with 2 mM L-glutamine (Sigma-Aldrich, Poole Dorset, UK), 15% FCS, and an antibiotic/antimycotic mixture (Sigma-Aldrich) (HCM, standard HEPES culture medium). Explants were allowed to equilibrate for a further 3 days before experimentation. For all investigations, control and experimental explants were obtained from the same donor to minimize interdonor variation.

### Laser Procedure

**Procedure Used for Assessment of Cellular Response to the Laser Treatment.** For studies involving cellular response to laser (apart from MMP release) and subsequent dynamics of RPE migration, potential areas for laser treatment were marked out on the explant with a 2-mm-diameter trephine**.** This was required to identify lasered areas for subsequent immunohistochemical analyses, as the laser energies used were below visual threshold. The control group went through the same marking procedure but without laser irradiation. Thus, on day 4 of culture, having selected areas for laser treatment, the incubation medium (HCM) was replaced with sterile phenol red-free Hank's balanced salt solution (HBSS; Sigma-Aldrich, UK) and explants transported to the laser room. The control organ cultures remained with the laser-treated group throughout the procedure.

RPE-BC organ cultures were irradiated with an Ellex 2RT 3-ns pulse laser system (Ellex Medical Pty, Adelaide, Australia). This specially designed prototype model operates a Q-switched frequency doubled YAG (532 nm) laser, and is programmable to deliver one or a series of 3-ns pulses with a discontinuous energy beam profile.

The laser treatment was performed using the clinical slit-lamp delivery system of a conventional YAG laser (UltraQ, Ellex Medical). The culture dishes retaining the RPE-BC organ cultures were positioned on a specially designed sample holder that rested in place of the chin-rest of the slit lamp. A front surface coated mirror at 45° angle was carefully aligned to deflect the treatment beam vertically onto the specimen.

In the experimental samples, each 2-mm-diameter marked area received a total of 3 to 6 separate exposures, 400 μm in diameter; energy delivered was 0.3 mJ per exposure or 240 mJ/cm$^2$. The 400-μm lesions were placed at the center, and in the surrounding region as follows: north, south, east, west, northwest, northeast, southwest, and southeast. A printed digital photograph was also marked as the laser lesions were delivered. It was therefore possible to keep track of the lesion sites during subsequent manipulation of the tissue sample. Care was taken to ensure proper focusing of the aiming beam on the surface of the RPE monolayer.

Following laser treatment, all samples were transported back to the tissue culture room and the HBSS was replaced with the standard culture incubation medium described above. The procedural time from removal and transport of tissue, subsequent laser treatment, and re-introduction to the incubator rarely exceeded 30 minutes. Explants were generally maintained under tissue culture conditions for 0 to 14 days post laser treatment with medium being replenished every 2 to 4

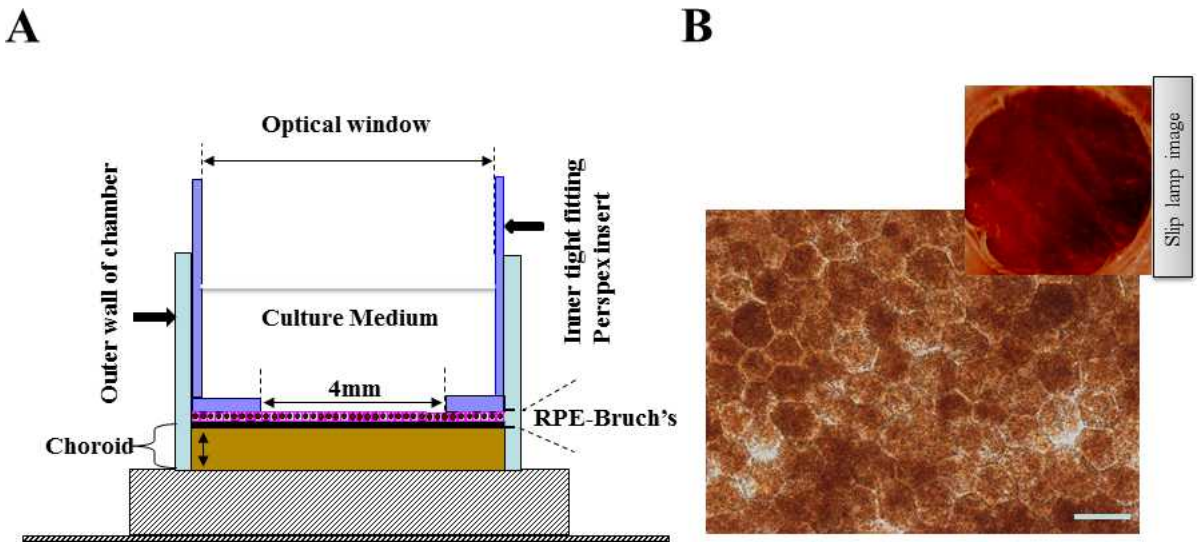


**Figure 1.** RPE-BC working model system. (**A**) Schematic of the tailor-made culture chamber for maintaining isolated RPE-BC organ cultures. After careful dissection, the 10-mm-diameter RPE-BC explant was positioned within the confines of the Perspex outer chamber wall with RPE cells facing uppermost. An inner tightly fitting Perspex insert with a 4-mm central aperture was then carefully lowered to tightly seal and clamp the preparation. Culture medium was added by initially pipetting over the lip of the inner insert so as to minimize any perturbation to the RPE monolayer. (**B**) Representative phase-contrast micrograph of a 14-day maintained explant clearly showing the confluent RPE monolayer and characteristic hexagonal phenotype. The insert is a low-power slit-lamp image of the same RPE preparation held within the confines of the chamber assembly. Bar: 20 μm.

days. At designated times, explants were removed and processed for immunohistochemical analyses.

**Procedure Used for Assessment of MMP Release Profiles Subsequent to the Laser Treatment.** For assessment of MMP release profiles, explants were not marked with the 2-mm-diameter trephine (to avoid nonspecific release of MMPs) but were irradiated with four randomly placed 400-μm spots followed by return to the 15% FCS supplemented HCM medium**.** This medium was replaced with one containing 1% FCS 24 hours before collection of medium for MMP analysis. This was deemed necessary to reduce the amount of MMPs from the FCS component so that the released RPE components could be accurately examined by the zymography procedure. Complete removal of FCS would have been ideal, but as we have previously demonstrated, this inhibits the release of MMPs by the RPE.[20] Incorporating 1% FCS restored the release profiles and the procedure was applied to both control and lasered samples.

Incubation medium was collected from both control and laser-treated organ cultures on days 0, 1, 2, 4, 7, and 14 post laser treatments.

## Assessment of Cellular Response to the Laser Treatment

A combination of techniques was used to assess cell viability, division, and proliferation in both control and lasered samples. The bromodeoxyuridine (BrdU) and mitochondrial enzyme (MTT) assays were performed by colorimetric estimation to evaluate the overall status of the tissue explants. More detailed microscopic investigations were undertaken in the marked regions of the explants with LIVE/DEAD and SYTOX assays. In these latter studies, antibodies to ZO-1 were also used to evaluate the integrity of RPE junctional complexes.

**BrdU Incorporation Assays.** The dividing/proliferating capacity of the RPE monolayer in control and laser treated explants was evaluated using a BrdU incorporation assay kit according the manufacturer's protocol (BrdU, Cell Proliferation Kit; Chemicon, Billerica, MA)**.**

Briefly, both groups of control and laser treated RPE-BC organ cultures (maintained in their respective tissue holders) were labeled with BrdU for 1 hour, washed with PBS, and reacted with anti-BrdU antibody (1:1000 dilution in PBS) for another 1 hour at room temperature. After washing twice with PBS, the secondary antibody (1:100 dilution) was added and allowed to incubate for 30 minutes. After another wash in PBS, the TMB peroxidase substrate was added and followed by a 30-minute incubation. Finally, 100 μL of this solution was carefully collected and transferred to a 96-well plate. The plates were analyzed with a colorimetric plate reader (model 450; BioRad, Hemel Hempstead, Hertfordshire, UK) at 450 to 590 nm. Assays were performed on explants maintained for 0 to 30 days post laser treatment.

**MTT Cell Viability Assay.** The RPE-BC organ cultures were washed with PBS and then incubated at 37°C for 4 hours with the MTT reagent**.** They were then washed and the RPE cells and the precipitated formazan crystals were solubilized over 12 hours by adding 100 μL dimethyl sulfoxide into each well. The supernatant was then collected and transferred to a 96-well plate for measuring the absorbance on an ELISA plate reader with a test wavelength of 570 nm and a reference wavelength of 630 nm (OD570–OD630). Absorbance values for the freshly isolated explants were designated as 100% and viability levels for the other time periods (covering range 0–60 days) calculated accordingly.

**LIVE/DEAD Assays.** Viability of the RPE-BCM organ cultures was determined by Molecular Probes' LIVE/DEAD Viability/Cytotoxicity Kit (Sigma, L3224)**.** The kit contains two fluorescent probes that measure cell viability. Live cells exhibit green fluorescence because of the enzymatic conversion of the nonfluorescent, cell-permeable dye calcein AM to the intensely fluorescent calcein. LIVE/DEAD stain was prepared with 2 μM calcein AM and 4 μM EthD-1 in PBS. The samples were incubated with the dyes for 1 hour after which the excess dye solution was removed and 0.5 mL of fresh PBS was added for 30 minutes. Confocal microscopy was used to quantify the number of viable/dead cells in the tissue preparation.

**SYTOX Cell Death Assays.** RPE cell death was also assessed using the SYTOX cell death assay**.** SYTOX Orange (from Molecular Probes) is a DNA dye that can penetrate damaged plasma membranes to stain cellular nuclei.[43] The RPE-BC organ cultures were incubated in the dark with 5 nM SYTOX Orange for 15 minutes, followed by extensive washing to remove excess dye. SYTOX-positive (dead) cells were counted from 10 randomly chosen areas on each of 400-μm spots using

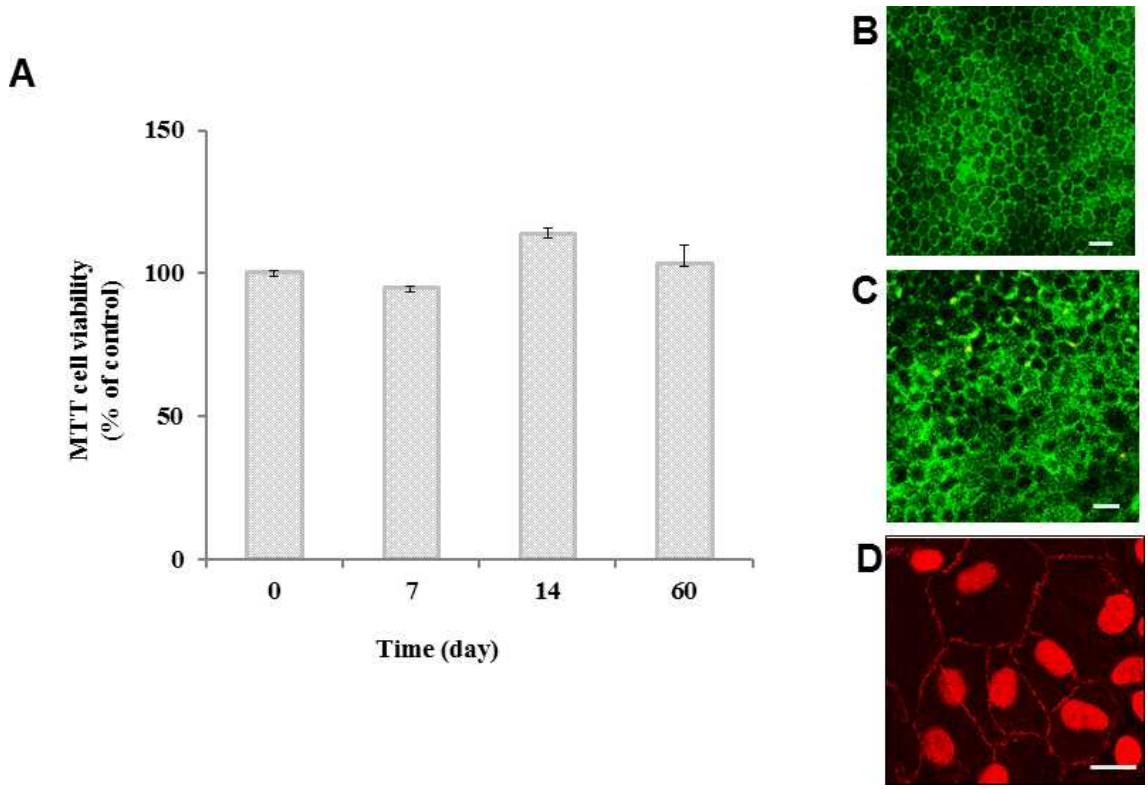


**Figure 2.** Viability assessment of human RPE cells in the RPE-BC working model system. A quantitative assessment of cellular viability was obtained with the MTT assay. The optical density of dissolved formazan in the freshly isolated preparations was taken as 100% live cells and compared with the optical densities obtained for cultures maintained for 7, 14, and 60 days (**A**). Under the culture conditions, RPE cells could be maintained up to the 60th day of incubation. Data are presented as mean ± SEM of 3 to 6 preparations. The LIVE/DEAD assay of a representative 14-day (**B**) and 3-week cultured explant (**C**) showed widespread green fluorescence on the confocal image, indicative of a confluent RPE layer (Bar: 25 μm). The intactness of RPE junctional complexes was assessed using antibodies to the ZO-1 junctional protein. (**D**) As the fluorescent image demonstrates, in a 3-week incubated preparation, continuous rings of junctional proteins were localized around the periphery of individual RPE cells, indicative of good barrier function. The cells were counterstained with Propidium iodide, a nuclear DNA stain. Bar: 10 μm.

a fluorescence microscope (Nikon Eclipse E600, Nikon, Japan) with a ×20 objective, and the ratio of dead to total cells determined.

**Immunocytochemistry for ZO-1 AND F-ACTIN.** RPE-BC organ culture chambers were uncoupled at various time periods following laser treatment and incubated in 4.0% paraformaldehyde (in PBS) overnight at 4°C. RPE cells were permeabilized (dependent on the experiments) in 0.5% Triton X-100 (in PBS) for 10 minutes and then incubated with primary mouse antibodies to ZO-1 (Zymed Laboratories Inc., San Francisco, CA), supplemented with 1.0 mg/mL BSA at 4°C. After rinsing, the preparations were incubated with the appropriate FITC conjugated secondary antibody for detection of ZO-1 (Jackson ImmunoResearch Laboratories, West Grove, PA) diluted 1:500 in PBS.

F-actin was visualized by treatment of fixed cells for 30 minutes at room temperature with fluorescent-conjugated Phalloidin (Sigma-Aldrich, UK).

**Substrate-Gel-Electrophoresis (Zymography).** The proteolytic activity of MMP-2 and MMP-9 released by RPE cells into the incubation medium in control and lasered preparations was assayed with gelatin zymography as described elsewhere.[19] Briefly, RPE-conditioned growth medium was diluted (1:1 vol/vol) in Novex tris-glycerine SDS buffer (Invitrogen, UK) and incubated at room temperature for 15 minutes. Twenty micro liters of each sample were loaded into the wells of Novex 10% gelatin Zymogram gels (Invitrogen, UK). The gels were subjected to electrophoresis for 90 minutes at 125 V at 4°C. The gels were then uncoupled from their holding container, washed for 1 hour in 2.5% Triton X-100 solution, washed again in ddH2O and incubated at 37°C overnight in developing buffer (Invitrogen, UK). Following this incubation period, the gels were washed several times with $ddH_2O$ and stained for 3 hours at room temperature with Simply Blue Safe stain (Invitrogen). Areas of protease activity appeared as clear bands against a dark blue background. The proteolytic activity of MMPs as opposed to other nonspecific proteases was confirmed by incubating some gels in incubation buffer containing 20 mM EDTA (data not shown).

The Zymograms were then washed several times with water, scanned at high resolution (G800 model, BioRad UK) and data stored in TIFF format. After gray-scale inversion of the original gel scans, the resultant images were imported into an image analysis program for analysis and quantification (Quantiscan for Windows; Biosoft, Cambridge, UK).

The band intensity values of each apparent band were corrected for background staining for each gel. Pixel analysis was used to generate a graph of intensity and allowed the area under the curve to be calculated. By incorporating the standard in the gel together with the FCS sample and by normalizing staining intensity, MMP bands obtained from different experiments and different gels could be compared.

## Statistical Methods

Data were expressed as mean ± SEM resulting from 3 to 10 independent series of experiments with each experiment performed in duplicate. Statistical analysis was performed using the nonparametric Mann-Whitney test to assess significant differences ($P < 0.05$; $P < 0.01$ or $P < 0.001$) between control and lasered samples using the add-in XLSTAT statistical analysis software (Addinsoft, New York, NY) for Microsoft Excel.

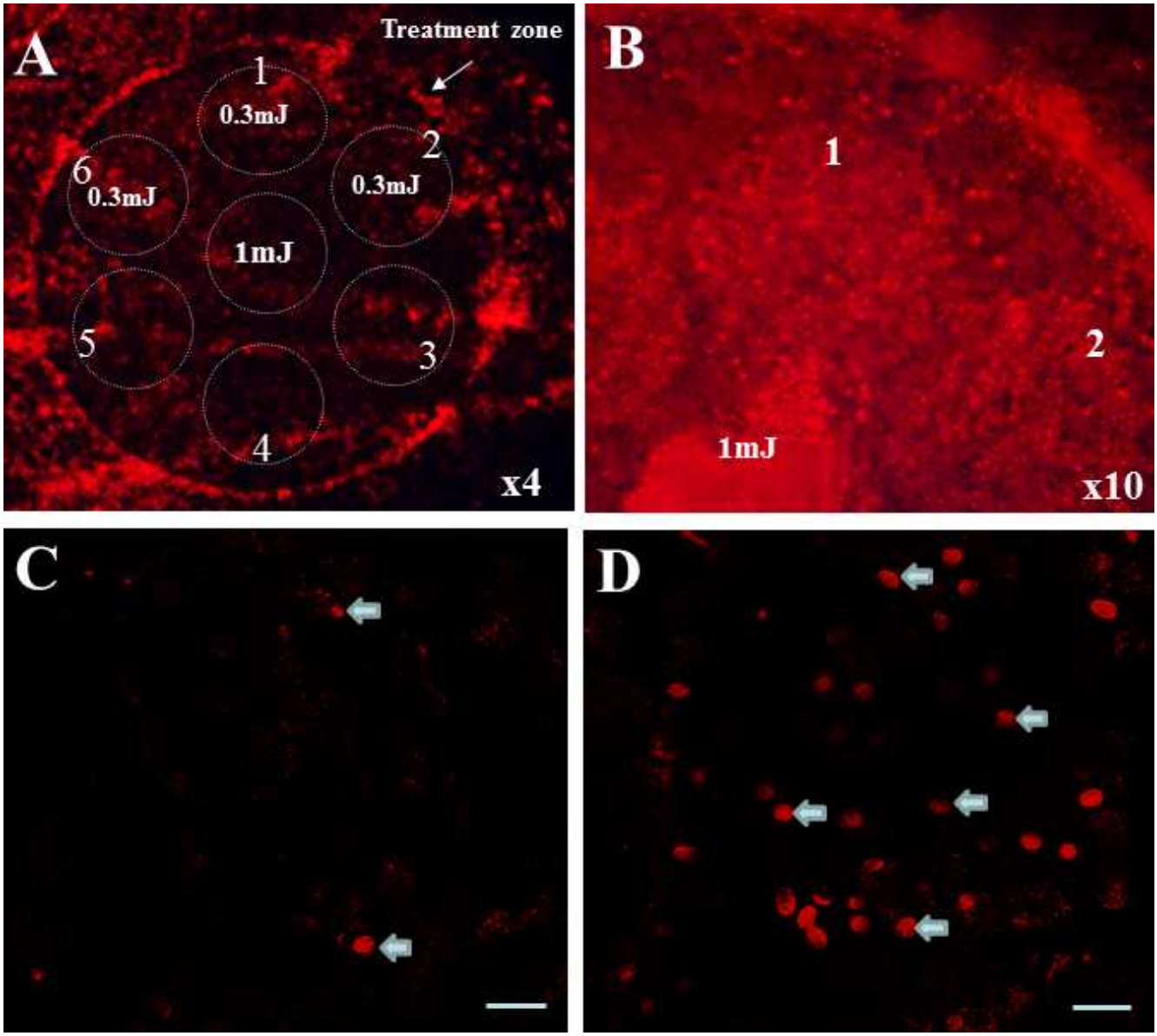


**Figure 3.** Surface morphology of laser-treated explants. The figure illustrates a typical laser experiment. Within the selected 2-mm-diameter treatment zone, six "burns" were placed on the inner border of the target area, each at an energy level of 0.3 mJ/"burn," total energy delivery of 240 mJ/cm$^2$. For comparative purposes, one central burn of higher energy (1 mJ/"burn," total energy 800 mJ/cm$^2$) was also incorporated (**A**). (**B**) Higher magnification photographs of the central 1-mJ and lasered regions 1 and 2 after laser. Lasered regions showed a slightly paler coloration compared with nonirradiated areas. In comparison, the higher-energy lesion (1 mJ) resulted in the virtual clearing of all RPE cells from the treated area. (**C**, **D**) Confocal images of SYTOX Orange–stained control and lasered regions, respectively. Lasered region showed the random distribution of damaged RPE cells rather than clusters. Bars: 10 μm.

## Results

### Stability of the Human RPE-BC Organ Culture System

Most of the explants (>80%) initiated into the culture protocol showed the characteristic RPE mosaiclike morphological appearance and remained fully confluent on day 3 of the examination. These were used in the experimental studies, the remainder being discarded. A representative slit-lamp image (insert, Fig. 1B) and higher magnification (Fig. 1B) of a 14-day maintained explant shows the confluent RPE monolayer and hexagonal epithelial phenotype.

Similarly, the MTT viability assay, spanning a culture period of 0 to 60 days demonstrated the stability of the RPE monolayer (Fig. 2A). At the seventh day assessment point, cell density (being proportional to the absorbance of the solubilized formazan) was slightly reduced to 94.5% ± 1.2% (mean ± SEM, $n \geq 3$) of the freshly initiated explant. This slight drop, although not significant, may be related to tissue manipulation at dissection, postmortem procedures, and other stabilization in situ factors. Cultures maintained up to the 60th day of assessment displayed cell densities that were similar to the freshly introduced explants (103.3% ± 6.8%).

Representative LIVE/DEAD viability assays conducted at day 14 (Fig. 2B) and 3 weeks into culture (Fig. 2C) were dominated by the green fluorescence of live cells, indicative of a confluent

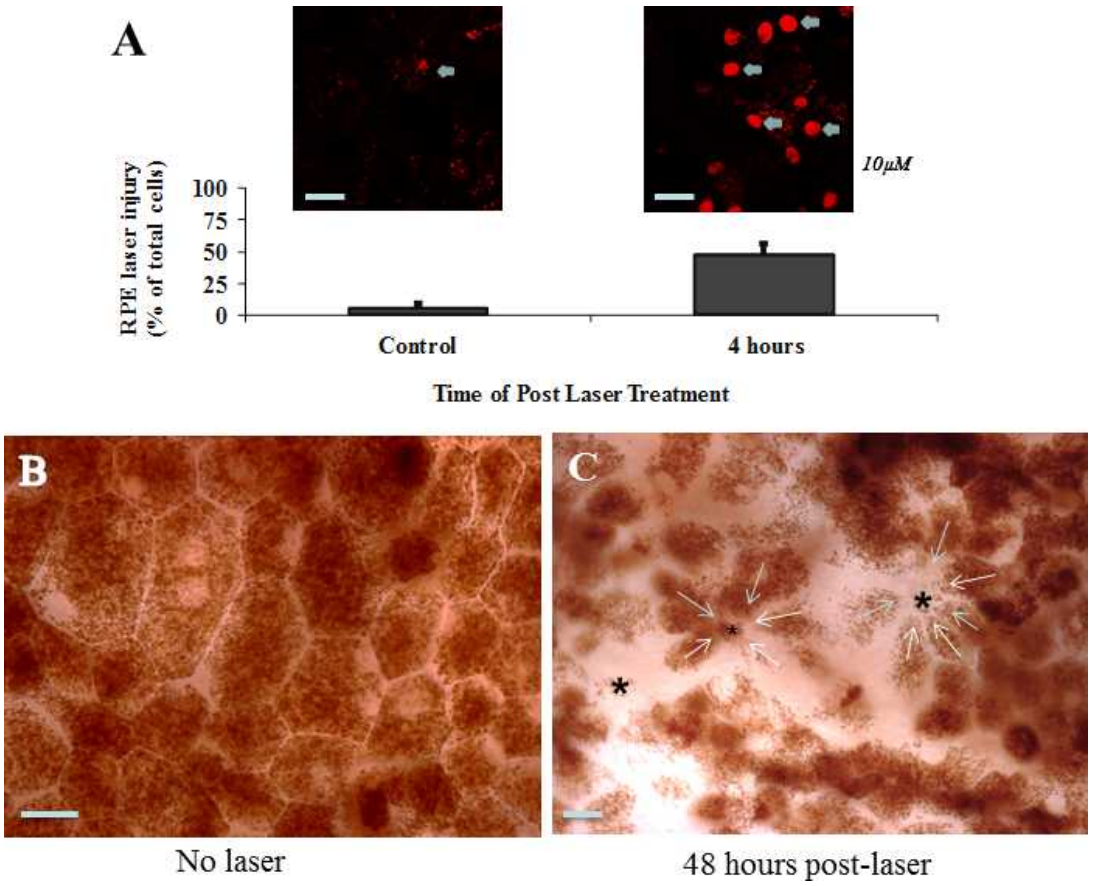


**Figure 4.** Assessment of laser-induced cell death. (**A**) Representative micrographs of control and 4-hour post laser organ cultures fixed and labeled with SYTOX Orange dye. The percentage of dead cells (identified by SYTOX staining) was determined across several fields within the lasered zone and shown in the bar graphs as mean ± SEM, $n = 6$ (Bar: 10 μm). (**B**, **C**) Control RPE monolayer and lasered region irradiated with 0.3 mJ after 48 hours. This region shows loss of many RPE cells (three identified with asterisks). An early recovery phase is apparent with elongated RPE cells migrating to resurface the vacant areas within the lesion. Bars: 10 μm.

RPE layer. The integrity of intercellular junctions between RPE cells was monitored by examining the expression of the junction-associated protein ZO-1. The fluorescent image of Figure 2D, taken from an explant maintained for 3 weeks, demonstrates intense staining of peripheral borders of RPE cells, indicative of good barrier function at this time period.

## Laser Effects on RPE Dynamics

In the laser studies, several (three to six) 400-μm diameter lesions were placed within the 2-mm diameter selected zone and a representative placing is shown in Figure 3A. In this illustrative example, six exposures were placed on the inner border of the target area, each with a total energy of 0.3 mJ or 240 mJ/cm$^2$. For comparative purposes, one central exposure of higher energy (1 mJ/ or 800 mJ/cm$^2$) was also incorporated.

Some of the explants were examined 4 hours after laser treatment. Regions irradiated with 0.3 mJ per exposure showed a paler coloration compared with the nonirradiated adjacent areas and this was most likely a result of the destruction of the melanin component of RPE cells (Fig. 3B). Total laser energy of 1 mJ was associated with complete removal of all RPE cells within the irradiated zone (Fig. 3B). SYTOX Orange staining was used to assess the spatial distribution of damaged RPE cells. In control regions, only occasional damaged RPE cells were identified (Fig. 3C). Irradiation with 0.3 mJ was associated with a random distribution of damaged RPE cells within the irradiated zone (Fig. 3D). Further quantitative studies incorporating the SYTOX assay showed that the laser treatment (0.3 mJ) was associated with loss of 47% ± 8% (mean ± SEM, $n = 6$) of RPE cells compared with 6% ± 4% (mean ± SEM, $n = 6$) for the control regions (Fig. 4A).

After 48 hours following the laser treatment with energies of 0.3 mJ, the loss of individual RPE cells becomes clearly evident (Fig. 4C). RPE cells adjacent to the vacant spaces displayed elongated profiles as they attempted to resurface the damaged areas (indicated by arrows in Fig. 4C). In regions with loss of solitary or a small group of RPE cells, repopulation by the movement and enlargement of neighboring cells resulted in rapid closure of the wound within 7 days of the laser treatment (Fig. 5A). In areas of greater cell loss (>10–30 RPE cells), the regenerative phase usually started at the periphery of the lesion with migration toward the wound center, resulting in resurfacing of the wound bed over 10 to 14 days (Fig. 5B and insert). By day 14 posttreatment, even the larger injured beds were covered by a continuous monolayer and the RPE cytoskeleton (as assessed by actin localization) displayed the typical circumferential ring organization usually associated with mature epithelial cells (Fig. 5C).

The degree of cell division/proliferation in both control and laser-treated groups was quantified with the BrdU incorporation assay. Although both control and treated groups showed a time-dependent increase in BrdU incorporation, that in the treated groups was much elevated. Thus after 7 days in culture, control explants showed an increase of optical density from a baseline at 0 days of 1.15 ± 0.26 to 1.31 ± 0.22 (NS) whereas

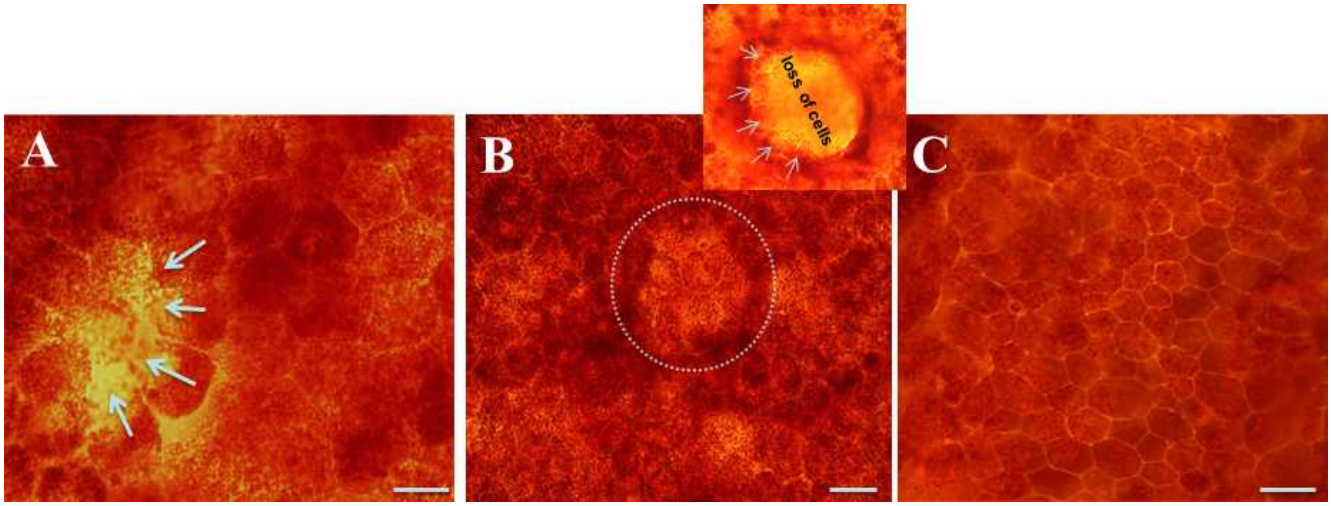


**Figure 5.** Assessment of the regenerative potential of the RPE monolayer subject to laser irradiation. (**A**) Representative phase-contrast micrograph where regions with loss of solitary or a small group of RPE cells were repopulated within 7 days of the laser treatment. The elongation of the surrounding RPE cells and their direction of migration is shown by the arrows. In areas of greater loss (>10–30 RPE cells), the regenerative phase usually started at the periphery of the lesion with migration toward the wound center (**B**, and insert). This recovery resulted in resurfacing of the wound bed over 10 to 14 days. By day 14 posttreatment, even the larger injured beds were covered by a continuous monolayer and the RPE cytoskeleton (as assessed by actin localization using TRITC-Phalloidin) displayed the typical circumferential ring organization usually associated with mature epithelial cells (**C**). Bars: 20 μm.

laser-treated samples showed an optical density increase to 2.21 ± 0.07 (Fig. 6; $P < 0.05$). Even at day 14, the difference in BrdU incorporation was still maintained ($P < 0.05$). By post laser day 30, BrdU incorporation in the lasered samples had decreased to basal control values.

## MMP Release Pattern Following the Laser Treatment

RPE dependent release of MMPs into the culture medium was followed over 0 to 14 days in both control and laser-treated explants. Representative zymograms showing the distribution patterns of MMP species under these experimental regimes is given in Figures 7A and 7B.

In the control explants, release of pro-MMP-9 was barely discernable and was without time-dependent alterations during the course of the incubation period (Fig. 7A). Active forms of MMP-9 were never observed in these samples. In sharp contrast, pro-MMP-2 was expressed robustly with the occasional presence of active forms of the enzyme.

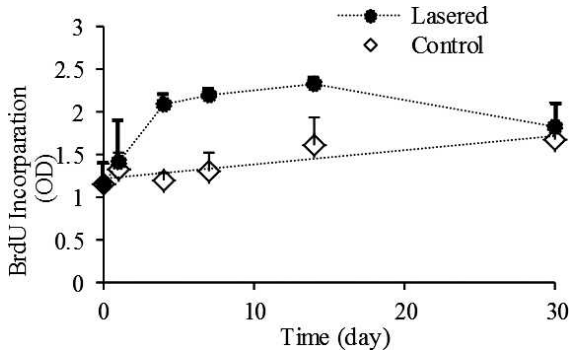


**Figure 6.** RPE cell proliferation in control and lasered explants. The degree of cell division/proliferation in both control (*open circles*) and laser treated (*filled circles*) groups was quantified with the BrdU incorporation assay. The control group of explants showed a linear increase in BrdU incorporation that was statistically significant ($P < 0.01$). However, the lasered samples showed a more rigorous increase with incorporation at days 4, 7, and 14 being considerably elevated compared with controls ($P < 0.05$). By day 30 of incubation, the levels between controls and treated samples were not significantly different. Data points are presented as mean ± SEM with $n = 3$ to 5 preparations.

However, following laser treatment, MMP expression patterns were dramatically altered (Figs. 7B–D). Level of pro-MMP-9 was significantly elevated nearly threefold by day 2 ($P < 0.05$) with levels remaining significantly elevated up to day 14 of experimentation. The earliest MMP response occurred within 4 hours of the laser with the appearance of the transitory intermediate (88 kDa) and the fully activated (82 kDa) form of active MMP-9. Because active MMP-9 was not present in the control incubations, the level present at 4 hours in the lasered samples was taken to represent the value at day 0 to allow comparison with subsequent incubation periods. Levels of active MMP-9 progressively increased reaching a 4.4-fold high by day 7 ($P < 0.01$). As with pro-MMP-9, active MMP-9 levels at day 14 were lower than at day 7 but nonetheless still statistically elevated compared with day 0.

Levels of pro-MMP-2 after the laser treatment were not significantly different from controls, whereas changes in active MMP-2 were qualitatively similar to those observed for active MMP-9 (Figs. 7B–D). Thus, active MMP-2 levels increased up to day 7 (6.7-fold) with levels at day 14 being reduced (3.4-fold) but still remaining elevated ($P < 0.001$) compared with day 0.

## Discussion

The first priority of the study was to demonstrate the stability of the in vitro RPE-Bruch's choroid organ culture system so that the effects of subsequent laser intervention could be interpreted correctly. A 3-day preliminary incubation period was incorporated so that explants showing a confluent RPE layer with hexagonal phenotypic characteristics (representing 80% of samples) could be initiated into the study.

Several tests were used to assess the viability and stability of these explants. Although our experimental protocol was restricted to 0 to 14 days post laser treatment, explant viability assessments were performed for much longer periods. Calcein-AM staining of day 14 and 3-week old explants showed the

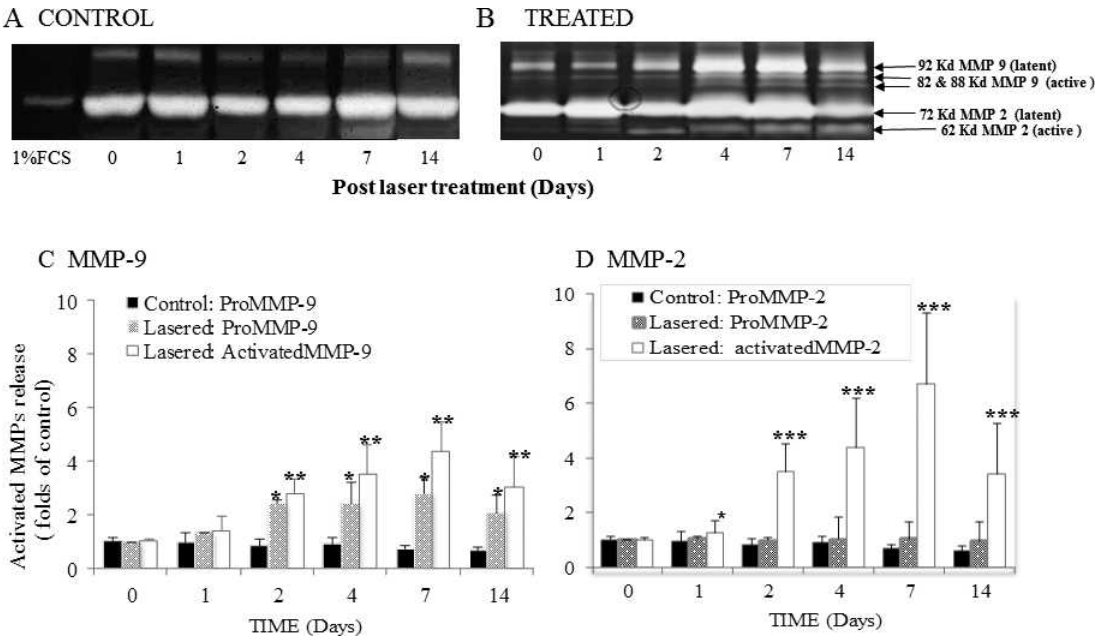


**Figure 7.** Laser-mediated alterations in the release profiles of MMP-2 and MMP-9. Gelatine zymograms showing the release of MMP-2 and MMP-9 from control and lasered explants maintained for 14 days are shown in (**A**) and (**B**), respectively. MMP release from control explants was characterized by low levels of pro-MMP-9, absent levels of active MMP-9, considerable output of pro-MMP-2, and the occasional presence of active MMP-2. Laser irradiation was associated with a progressive increase in levels of active MMP-9 and pro-MMP-2 and pro-MMP-9 up to the seventh day of measurement. Level of these species was reduced at the 14th day of measurement (in comparison with level at day 7) but remained statistically elevated compared with controls. Levels of pro-MMP-2 were not altered. (**C**, **D**) The time course of MMP changes is represented by the bar graphs. The bar graphs are mean ± SEM with $n = 6$ for controls and $n = 4$ to 6 for lasered samples. $^{*}P < 0.05$; $^{**}P < 0.01$; $^{***}P < 0.001$.

predominant green fluorescence of live cells. Identifying a small number of dead cells in a predominantly live cell population with this stain was difficult. The alternative SYTOX Orange dye, specifically targeting dead cells, showed the occasional presence of solitary dead cells; clusters of dead RPE cells were never observed.

It is possible that over the culture period, as dead cells were lost into the medium, remaining cells proliferated to maintain the confluency of the preparation. This may have occurred to a minor degree, as the BrdU incorporation assay for proliferating cells showed a statistically significant increase ($P < 0.01$) in control explants over the incubation period of 0 to 30 days; however, the magnitude of this input would have been minimal, as the release of pro-MMP-2 and pro-MMP-9 into the medium remained at the basal level throughout the 14-day observation period. A disturbance in the MMP release pool or additional secretion of active MMPs would be indicative of cellular mobilization and rearrangement, a feature not encountered in the control explants.[20]

In addition to the viability assessment, immunostaining for the junctional protein ZO-1, carried out at 3 weeks of incubation, showed the RPE barrier to have remained intact. Thus, the laser experiments were undertaken with a viable and characterized RPE-Bruch's-choroid organ culture system.

Other studies using porcine tissue have shown that 5-μs-duration pulses obtained from an argon laser (514 nm) with an energy density of 256 mJ/cm$^2$ were without damage to the RPE, although 2.5% of pulses were associated with microbubble formation.[44] It is suggested that the formation of small or fewer microbubbles may not have allowed sufficient volume expansion to disrupt intracellular structures. However, energy levels of 440 mJ/cm$^2$ resulted in 100% of RPE cells being damaged. These authors have also shown considerable variation in RPE damage thresholds ($ED_{50}$ = 252 mJ/cm$^2$, $ED_{15}$ = 166 mJ/cm$^2$, and $ED_{85}$ = 359 mJ/cm$^2$) and suggest this to be a result of RPE donor variation in the level of pigmentation. Other studies with microsecond pulses and using porcine RPE have shown comparable damage thresholds.[45] In one human study, using a Nd:YLF laser operating at a wavelength of 527 nm, RPE damage thresholds ($ED_{50}$) were much lower with 200-ns pulse widths (317 mJ/cm$^2$) compared with the 1.7-ms pulses (625 mJ/cm$^2$).[33]

In the present study, nonvisible RPE lesions were delivered with an Ellex system incorporating a Q-switched frequency doubled YAG laser (532 nm) and pulses of 3-ns duration. At an irradiance of 240 mJ/cm$^2$, RPE loss was determined to be 47% ± 8 %, compatible with the studies cited earlier. Higher energy levels of 800 mJ/cm$^2$ were associated with the complete clearance of all RPE cells within the lesion zone.

At the 4-hour examination period, some RPE cells were lost, whereas others showed membrane damage and structural disintegration. Regions with the loss of solitary or a small group of RPE cells were rapidly repopulated within 7 days of the laser treatment. With larger areas of cellular loss (10–30 cells), the regenerative phase was observed to start at the periphery of the localized lesion with migration and proliferation toward the wound center, with resurfacing being completed within 10 to 14 days. This proliferative phase to repopulate damaged RPE beds was confirmed by the increase in BrdU incorporation with levels of 102.1% ± 11.1% over controls at day 7 ($P < 0.05$) and maintained until day 14 of examination followed by return to baseline by day 30. Thus, although morphological examination suggested repopulation of beds by days 10 to 14, clearly underlying adjustments were still ongoing for much longer periods. Further work is required to quantify the relative contribution of migration and proliferation to wound closure and could be undertaken using the proliferative inhibitor, 5-fluorouracil.

Laser treatment dramatically altered the basal release profiles of MMPs by the RPE. Copious amounts of both pro-

and active MMP-9 species increased progressively up to the seventh day of observation. Although levels were reduced by day 14 in comparison with day 7, they were still much elevated, supporting the results of the BrdU incorporation time profile. Similarly, levels of active MMP-2 increased rapidly with a similar time course to that of active MMP-9. The time for peak response in the active MMP profiles cannot be ascertained in the present study, as periods between days 7 and 14 were not sampled. Nonetheless, the profiles of Figures 7C and 7D suggest a downward trend by day 14 of laser exposure. Other workers, using pan-retinal photocoagulation of human RPE explants, have also shown increased cellular proliferation and concomitant changes in MMPs.[46] Further work is required to extend our observation period so that the declining phase of the MMP response can be fully quantified.

Previous work with human cell lines and primary cultures has shown a cell-cycle dependent release of active MMP-2 and MMP-9.[20] In this well-defined system with cell-cycle synchronization, active MMP-9 release was terminated near half confluence with active MMP-2 being expressed thereafter. In the present laser studies, the changes in active MMP-2 and MMP-9 occurred in tandem with levels remaining high despite visual closure of the wound. One reason for the discrepancy may be that in the laser studies, because of the varied distribution in damaged RPE clusters, the MMP response would not be synchronized, producing the average profile given in Figure 7. Nonetheless, in these studies, the MMP response was maintained well after closure of the wound.

The importance of laser-mediated increase in expression of activated MMPs relates to their likely effects on underlying Bruch's membrane. Aging of human Bruch's is associated with gross structural alterations and deposition of debris, culminating in functional decline.[1,10,11,47] The accumulation of large amounts of denatured collagen together with the conspicuous reduction in activated MMPs (particularly in the macular region) has suggested the presence of abnormalities in the MMP degradation system of the membrane.[3,18] In the advanced aging of Bruch's associated with ARMD, the severe decline in functional competence is thought to undermine the nutritional transport status of the membrane, leading to the death of RPE and photoreceptor cells of the retina.[12,13] Therefore, therapeutic intervention to improve the transport characteristics of Bruch's membrane remains a viable option for addressing ARMD. As already mentioned, exogenous delivery of active MMPs to donor Bruch's was shown to improve the transport characteristics of the membrane.[20]

The different rates of RPE repopulation dependent on the size of the localized lesion have an important bearing for futuristic clinical transference of the laser technique. When a large group of RPE cells is damaged, recovery begins at the periphery, with wound closure taking 10 to 14 days. During this period, photoreceptors at the wound center would be without RPE support and would therefore be exposed to an increased risk of damage. To minimize the likelihood of photoreceptor damage, the knockout of solitary or small groups of RPE cells within the lesion zone would lead to rapid repopulation, reducing the time over which photoreceptors remained without RPE support. Theoretically, this could be achieved with current lasers by reducing beam energies resulting in about 15% cellular knockout (i.e., using $ED_{15}$ values). However, as previous studies have demonstrated for porcine RPE, there was considerable variation in ED values. In humans, this regime would be further complicated by variations in pigment density among patients and across the fundus of individuals. The alternative would be to use slightly higher energies (to ensure RPE knockout) but with a speckled laser beam profile, as in the present study. Thus, individual or small groups of RPE cells would be targeted in a random spatial distribution within the lesion zone, allowing for rapid wound closure and considerably reduced risk of secondary receptor damage.

In summary, the use of short-pulsed lasers therefore provides a therapeutic vehicle for transiently increasing the level of active MMPs released by the RPE. Further work is required to assess the beneficial effect (if any) of such an enzymatic change on the functional properties of underlying Bruch's membrane.

## *References*


1. Marshall J, Hussain AA, Starita C, Moore DJ, Patmore A. Ageing and Bruch's membrane. In: Marmor MF, Wolfensberger TJ, eds. *Retinal Pigment Epithelium: Function and Disease*. New York, NY: Oxford University Press; 1998:669–692.
2. Curcio CA, Millican CL, Bailey T, Kruth HS. Accumulation of cholesterol with age in human Bruch's membrane. *Invest Ophthalmol Vis Sci*. 2001;42:265–274.
3. Karwatowski WSS, Jefferies TE, Duance VC, et al. Preparation of Bruch's membrane and analysis of the age related changes in the structural collagens. *Br J Ophthalmol*. 1995;79:944–952.
4. Handa JT, Verzijl N, Matsunaga H, et al. Increase in the advanced glycation end product pentosidine in Bruch's membrane with age. *Invest Ophthalmol Vis Sci*. 1999;40:775–779.
5. Hageman GS, Luthert PJ, Victor Chong NH, et al. An integrated hypothesis that considers drusen as biomarkers of immune-mediated processes at the RPE-Bruch's membrane interface in aging and age-related macular degeneration. *Prog Ret Eye Res*. 2001;20:705–732.
6. Hageman GS, Anderson DH, Johnson LV, et al. A common haplotype in the complement regulatory gene factor H (HFI/CFH) predisposes individuals to age-related macular degeneration. *Proc Natl Acad Sci U S A*. 2005;102:7227–7232.
7. Grindle CFJ, Marshall J. Ageing changes in Bruch's membrane and their functional implications. *Tans Opthalmol Soc U K*. 1978;98:172–175.
8. Bird AC, Marshall J. Retinal pigment epithelial detachments in the elderly. *Trans Ophthalmol Soc U K*. 1986;105:674–682.
9. Moore DJ, Hussain AA, Marshall J. Age-related variation in the hydraulic conductivity of Bruch's membrane. *Invest Ophthalmol Vis Sci*. 1995;36:1290–1297.
10. Starita C, Hussain AA, Pagliarini S, Marshall J. Hydrodynamics of ageing Bruch's membrane: implications for macular disease. *Exp Eye Res*. 1996;62:565–572.
11. Hussain AA, Rowe L, Marshall J. Age-related alterations in the diffusional transport of amino acids across the human Bruch's-choroid complex. *J Opt Soc Am A Opt Image Sci Vis*. 2002;19:166–172.
12. Hussain AA, Starita C, Marshall J. Transport characteristics of ageing human Bruch's membrane: implications for AMD. In: Loseliani OR, ed. *Focus on Macular Degeneration Research*. New York: Nova Biomedical Books; 2004;59–113.
13. Hussain AA, Starita C, Hodgetts A, Marshall J. Macromolecular diffusion characteristics of ageing human Bruch's membrane: implications for age-related macular degeneration (AMD). *Exp Eye Res*. 2010;90:703–710.
14. Brinckerhoff CE, Matrisian LM. Matrix metalloproteinases: a tail of a frog that became a prince. *Nat Rev Mol Cell Biol*. 2002;3:207–214.
15. Sternlicht MD, Werb Z. How matrix metalloproteinases regulate cell behavior. *Annu Rev Cell Dev Biol*. 2001;17:463–516.
16. McCawley LJ, Matrisian LM. Matrix metalloproteinases: they're not just for matrix anymore! *Curr Opin Cell Biol*. 2001;13:534–540.

17. Tjäderhane L, Larjava H, Sorsa T, et al. The activation and function of host matrix metalloproteinases in dentin matrix breakdown in caries lesions. *J Dent Res*. 1998;77:1622–1629.
18. Guo L, Hussain AA, Limb GA, Marshall J. Age-dependent variation in the metalloproteinase activity of isolated Bruch's membrane and choroid. *Invest Ophthalmol Vis Sci*. 1999;40: 2676–2682.
19. Hussain AA, Lee Y, Zhang JJ, Marshall J. Disturbed matrix metalloproteinase activity of Bruch's membrane in age-related macular degeneration (AMD). *Invest Ophthalmol Vis Sci*. 2011;52:4459–4466.
20. Ahir A, Guo L, Hussain AA, Marshall J. Expression of metalloproteinases from human retinal pigment epithelial cells and their effects on the hydraulic conductivity of Bruch's membrane. *Invest Ophthalmol Vis Sci*. 2002;43:458–465.
21. Gass JD. Drusen and disciform macular detachment and degeneration. *Arch Ophthalmol*. 1973;90:206–217.
22. Cleasby GW, Nakanishi AS, Norris JL. Prophylactic photocoagulation of the fellow eye in exudative senile maculopathy. A preliminary report. *Mod Probl Ophthalmol*. 1979;20:141–147.
23. Figueroa MS, Regueras A, Bertrand J. Laser photocoagulation to treat macular soft drusen in age-related macular degeneration. *Retina*. 1994;14:391–396.
24. Chen J, Fitzke F, Pauleikhoff D, Bird AC. Functional loss in age related Bruch's membrane change with a choroidal perfusion defect. *Invest Ophthalmol Vis Sci*. 1992;33:334–340.
25. Sunness JS, Johnson MA, Massof RW, Mercas S. Retinal sensitivity over drusen and non-drusen areas: a study using fundus perimetry. *Arch Ophthalmol*. 1988;106:1081–1084.
26. Mainster MA, White TJ, Tips JH, Wilson PW. Retinal-temperature increases produced by intense light sources. *J Opt Soc Am*. 1970;60:264–270.
27. Framme C, Walter A, Prahs P, et al. Structural changes of the retina after conventional laser photocoagulation and selective retina treatment (SRT) in spectral domain OCT. *Curr Eye Res*. 2009;34:568–579.
28. Choroidal Neovascularisation Prevention Trial Research Group. Laser treatment in eyes with large drusen: short-term effects seen in pilot randomized clinical trial. *Ophthalmology*. 1998;105:11–23.
29. Choroidal Neovascularisation Prevention Trial Research Group. Laser treatment in fellow eyes with large drusen. Updated findings from a pilot randomized clinical trial. *Ophthalmology*. 2003;110:971–978.
30. Friberg TR, Musch DC, Lim JI, et al. Prophylactic treatment of age-related macular degeneration report number 1: 810-nanometer laser to eyes with drusen. Unilaterally eligible patients. *Ophthalmology*. 2006;113:612–622.
31. Roider J, Hillenkamp F, Flotte T, Birngruber R. Microphotocoagulation: selective effects of repetitive short laser pulses. *Proc Natl Acad Sci U S A*. 1993;90:8643–8647.
32. Roegener J, Brinkmann R, Lin CP. Pump-probe detection of laser-induced microbubble formation in retinal pigment epithelium. *J Biomed Opt*. 2004;9:367–371.
33. Framme C, Wlaters A, Prahs P, Theisen-Kunde S, Brinkmann R. Comparison of threshold irradiances and online dosimetry for selective retina treatment (SRT) in patients treated with 200 nanoseconds and 1.7 microseconds laser pulses. *Lasers Surg Med*. 2008;40:616–624.
34. Brinkmann R, Hüttmann G, Rögener J, Roider J, Birngruber R, Lin CP. Origin of retinal pigment epithelium cell damage by pulsed laser irradiance in the nanosecond to microsecond time regimen. *Lasers Surg Med*. 2000;27:451–464.
35. Lin CP, Kelly MW. Cavitation and emission around laser-heated microparticles. *Appl Phys Lett*. 1998;72:1–3.
36. Framme C, Schuele G, Roider J, Birngruber R, Brinkmann R. Influence of pulse duration and pulse number in selective RPE laser treatment. *Lasers Surg Med*. 2004;34:206–215.
37. Brinkmann R, Roider J, Birngruber R. Selective retina therapy (SRT): a review on methods, techniques, preclinical and first clinical trials. *Bull Soc Belge Ophthalmol*. 2006;302:51–69.
38. Klatt C, Saeger M, Oppermann T, et al. Selective retina therapy for acute central serous chorioretinopathy. *Br J Ophthalmol*. 2011;95:83–88.
39. Casson RJ, Raymond G, Newland HS, Gilhotra JS, Gray TL. Pilot randomized trial of a nanopulse retinal laser versus conventional photocoagulation for the treatment of diabetic macular oedema [published online ahead of print February 2, 2012]. *Clin Experimen Ophthalmol*. doi: 10.1111/j.1442-9071.2012.02756.x.
40. Roider J, Brinkmann R, Wirbelauer C, Laqua H, Birngruber R. Subthreshold (retinal pigment epithelium) photocoagulation in macular diseases: a pilot study. *Br J Ophthalmol*. 2000;84: 40–47.
41. Wood JP, Plunkett M, Previn V, Chidlow G, Casson RJ. Nanosecond pulse lasers for retinal applications. *Lasers Surg Med*. 2011;43:499–510.
42. Hussain AA, Marshall J. Taurine transport pathways in the outer retina in relation to ageing and disease. In: Tombran-Tink J, Barnstable CJ, eds. *Ocular Transporters in Ophthalmic Diseases and Drug Delivery*. Totowa, NJ: Humana Press; 2008:217–235.
43. Matsuzaki T, Suzuki Fujikura K, Takata K. Nuclear staining for laser confocal microscopy. *Acta Histochem Cytochem*. 1997; 30:309–314.
44. Schuele G, Elsner H, Framme C, Roider J, Birngruber R, Brinkman R. Optoacoustic real-time dosimetry for selective retina treatment. *J Biomed Opt*. 2005;10:064022.
45. Roegener J, Brinkmann R, Lin CP. Pump-probe detection of laser-induced microbubble formation in retinal pigment epithelium. *J Biomed Opt*. 2004;9:367–371.
46. Flaxel C, Bradle J, Acott T, Samples JR. Retinal pigment epithelium produces matrix metalloproteinases after laser treatment. *Retina*. 2007;27:629–634.
47. Moore DJ, Clover GM. The effect of age on the macromolecular permeability of human Bruch's membrane. *Invest Ophthalmol Vis Sci*. 2001;42:2970–2975.